Free-carrier absorption in Be- and C-doped GaAs epilayers and far infrared detector applications

A. L. Korotkov, A. G. U. Perera,[a] and W. Z. Shen[b]
Department of Physics and Astronomy, Georgia State University, Atlanta, Georgia 30303

J. Herfort and K. H. Ploog
Paul-Drude Institut für Festkörperelektronik Hausvogteiplatz 5-7, 10117 Berlin, Germany

W. J. Schaff
School of Electrical Engineering, Cornell University, Ithaca, New York 14853

H. C. Liu
Institute for Microstructural Sciences, National Research Council, Ottawa K1A 0R6, Canada

(Received 15 September 2000; accepted for publication 14 December 2000)

Far infrared (FIR) absorption, reflection, and transmission in heavily doped p-GaAs multilayer structures have been measured for wavelengths 20–200 μm and compared with the calculated results. Both Be (in the range 3×10^{18}–$2.6\times10^{19}\,\mathrm{cm}^{-3}$) and C ($1.8\times10^{18}$–$4.7\times10^{19}\,\mathrm{cm}^{-3}$)-doped structures were studied. It is found that the observed absorption, reflection, and transmission are explained correctly by the model with a dominant role of free-carrier absorption in highly doped regions. High reflection from heavily doped thick layers is attractive for the resonant cavity enhanced FIR detectors. © *2001 American Institute of Physics.* [DOI: 10.1063/1.1347002]

I. INTRODUCTION

Most of the previous results[1,2] on optical absorption in p-GaAs were limited to relatively low doping concentrations $N_A \leqslant 10^{18}\,\mathrm{cm}^{-3}$. By means of molecular beam epitaxial (MBE) growth, higher hole concentrations up to $10^{20}\,\mathrm{cm}^{-3}$ are achievable.[3] Such a regime was studied in detail for wavelengths between 2 and 20 μm, where inter-valence-band transitions contribute significantly to the total absorption.[4] Free-carrier absorption measurements in the far infrared (FIR) range for $2\times10^{19}\,\mathrm{cm}^{-3}$ Be-doped GaAs epilayer were reported recently.[5] In this work FIR absorption by free holes in highly doped GaAs multilayer structures is investigated both experimentally and theoretically. This work, motivated by possible improvements in GaAs homojunction interfacial work-function internal photoemission (HIWIP) FIR detectors, concentrates on the FIR absorption and reflection of C-doped GaAs epilayers on an undoped GaAs substrate and Be-doped layers in multilayer GaAs structures. High performance FIR (40–200 μm) semiconductor detectors as well as large focal plane arrays are required for space astronomy applications, such as NASA's airborne mission, Stratospheric Observatory for Infrared Astronomy, and the European Space Agency's Far Infrared and Sub-mm Telescope programs. Si or GaAs HIWIP FIR detectors can compete with extrinsic Ge photoconductors (unstressed or stressed) and Ge blocked-impurity-band detectors due to the material advantage of Si or GaAs over Ge.[6] The cutoff wavelength λ_c is determined by the interfacial barrier height between the emitter layers and undoped intrinsic layers. Significant progress has already been achieved in the development of p-GaAs HIWIP FIR detectors,[7] resulting in a responsivity of 3.1 A/W and detectivity of $5.9\times10^{10}\,\mathrm{cm}\sqrt{\mathrm{Hz}}/\mathrm{W}$, with λ_c as long as 100 μm. The detection mechanism[6] of HIWIP detectors involves absorption in the highly doped emitter layers mainly by free carriers followed by the internal photoemission of photoexcited carriers across the junction barrier and then collection, hence the study of free-carrier absorption in multilayer GaAs structure looks like a way to improve the HIWIP performance.

II. EXPERIMENT

Three sets of samples were used for the reflection/absorption measurements. The first set, 280-nm-thick C-doped p-type GaAs layers used in this study were grown by MBE on 350-μm-thick semi-insulating GaAs (100) substrates, following a 200-nm-thick undoped GaAs buffer layer. The substrate temperature was kept at 500 and 580 °C for the doped and the buffer layers, respectively. The As_4-to-Ga beam equivalent ratio was kept constant at a value of 20. Carbon was used as a dopant in this set of GaAs samples since it allows a higher level of doping in comparison with beryllium concentration, which is limited to $(4-8)\times10^{18}\,\mathrm{cm}^{-3}$: higher level is necessary to extend the cutoff wavelength λ_c of the HIWIP detector to 200 μm and beyond.[7] Five samples with different concentrations in the epilayers (see Table I), and a piece of the substrate material as the reference were measured.

The second set of three multilayer structures was designed and grown by MBE as FIR HIWIP detectors. The substrate temperature was kept at 560 °C. The MBE epilayers consist of a bottom contact layer of thickness W_b, an undoped layer (W_{bi}), N periods of thin emitter (p^+) layer

[a]Electronic mail: uperera@gsu.edu
[b]Current address: Department of Applied Physics, Shanghai Jiao Tong University, 1954 Hua Shan Road, Shanghai 200030, People's Republic of China.

 © 2001 American Institute of Physics

Downloaded 29 Mar 2001 to 131.96.4.154. Redistribution subject to AIP copyright, see http://ojps.aip.org/japo/japcr.jsp

TABLE I. Parameters for five 280-nm-thick *C*-doped *p*-type GaAs epilayers with a 200-nm-thick undoped GaAs buffer layer, separating the 350-μm-thick semi-insulating GaAs (100) substrate. Doping concentration and relaxation time constant (τ) were estimated from the measured Hall coefficients and resistivities. The values for τ used for fitting the experimental spectral data are slightly lower than measured values. However, the tendency of decreasing τ with increasing concentration is very similar.

Sample No.	N_p (cm^{-3})	Measured τ (s)	Fitting τ (s)
M7.228	4.7×10^{19}	1.3×10^{-14}	1.2×10^{-14}
M7.227	2.4×10^{19}	1.6×10^{-14}	1.4×10^{-14}
M7.229	1.3×10^{19}	1.8×10^{-14}	1.5×10^{-14}
M7.270	5.9×10^{18}	2.5×10^{-14}	1.8×10^{-14}
M7.232	1.8×10^{18}	2.8×10^{-14}	2.0×10^{-14}

(W_e), and undoped intrinsic (i) layer (W_i), and finally a top emitter layer ($W_{\rm te}$) and a top contact layer ($W_{\rm tc}$). The emitter and contact layers were doped with beryllium. The doping concentration in emitters (N_e) was $(3-8)\times10^{18}\,\mathrm{cm}^{-3}$. The bottom and top contact layers were doped to (1.0–2.6) $\times10^{19}\,\mathrm{cm}^{-3}$. The layer parameters, measured by secondary ion mass spectroscopy (SIMS), are presented in Table II.

The third sample set consisted of the same structures as the second set, but the top contact layer was etched out completely, and the top emitter layer was also partially etched out, to obtain a set of samples as close to the detector structures shown in the bottom right corner of Fig. 4, in order to model the absorption process in the detector.

The spectra of absorption and transmission were taken with a Perkin-Elmer system 2000 Fourier transform infrared spectrometer at room temperature with a resolution of 4 cm^{-1}. The absorption in the whole structure (absorbed power normalized by the incident power) was calculated using the fact that the sum of the normalized reflection, transmission, and absorption should be unity.

III. THEORY

The free-carrier absorption in a p-type GaAs thin layer on an undoped GaAs substrate is calculated from the complex permittivity ϵ of the layer and the substrate. It is considered that free-carrier absorption is determined by the concentration and the relaxation time irrespective of the doping element (carbon or beryllium). In the reststrahlen region the frequency-dependent permittivity of the highly doped emitter layer can be considered as[8]

$$\epsilon=\epsilon_\infty\left(1-\frac{\omega_p^2}{\omega(\omega+i\omega_0)}\right)+\frac{\omega_{\rm TO}^2(\epsilon_s-\epsilon_\infty)}{\omega_{\rm TO}^2-\omega^2-i\gamma_p\omega}. \quad (1)$$

This expression does not take into account the multiphonon effects and oversimplifies the coupling of plasmons and phonons.[9] However, it has been used as the basis for sorting out plasmon-phonon effects, in several GaAs investigations.[8,10] The first term in Eq. (1) describes the free-carrier absorption in the frame of Drude model. Here ω is the optical frequency, $\omega_0=1/\tau$ is the free-carrier damping constant with relaxation time τ (which is independent of frequency in semiclassical transport theory), $\omega_p=(N_pq^2/\epsilon_0\epsilon_sm^*)^{1/2}$ is the plasma frequency, and ϵ_s is the low frequency dielectric constant of an intrinsic semiconductor, $m^*=0.5m_0$ is the heavy-hole effective mass in GaAs (in one-band model), m_0 is the free electron mass, and q is the magnitude of the electron charge. The carrier concentration N_p can be estimated from the doping level. The relaxation time τ is estimated using mobility measurements for C-doped samples (see Table I). For Be-doped samples τ is taken to be $\sim10^{-14}\,$s based on measurements done on similar (Be) doping level samples.[4] The ''reststrahlen'' term (the second term) in Eq. (1) describes the interaction with optical phonons in the Lorenz model. Here ϵ_s and ϵ_∞ are the ''static'' and ''high frequency'' dielectric constants, $\omega_{\rm TO}$ is the transverse optical-phonon frequency, and γ_p is a damping coefficient with dimension of frequency. The values for the parameters used are: $\hbar\omega_{\rm TO}=33.25\,$meV, $\epsilon_s=12.85$, $\epsilon_\infty=10.88(300\,\mathrm{K})$, $\hbar\gamma_p=0.25\,\mathrm{meV}$[8]. The permittivity of the substrate was calculated using Eq. (1) with values for carrier concentration $N_p=10^{15}\,\mathrm{cm}^{-3}$, and relaxation time $\tau=10^{-13}\,$s. At helium temperature the substrate and i regions may be described by only the reststrahlen term due to practically zero carrier concentration, and may be considered as transparent outside the reststrahlen region.

For the normal incidence of a plane electromagnetic wave, the solution of Maxwell's equations for the electric and magnetic fields inside each layer is the superposition of two plane waves, propagating in the opposite directions. The amplitudes of these waves can be found by matching electric

TABLE II. Parameters for three nonetched (set 2) and three etched (set 3) Be-doped p-GaAs HIWIP FIR detector structures. Here, $W_{\rm bc}$, $W_{\rm bi}$, W_e, W_i, $W_{\rm te}$, and $W_{\rm tc}$ are the thicknesses of the bottom contact (p^{++}), bottom intrinsic (i), emitter (p^+), intrinsic (i), top emitter (p^+), and top contact (p^{++}), respectively. N_c, N_e, and $N_{\rm te}$ are the doping concentrations of the contact, emitter and top emitter layers, respectively.

Sample No.	$W_{\rm bc}$ (nm)	N_c (10^{19} cm^{-3})	$W_{\rm bi}$ (nm)	No. of repeats N	W_e (nm)	N_e (10^{19} cm^{-3})	W_i (nm)	$W_{\rm te}$ (10^{19} cm^{-3})	$N_{\rm te}$ (nm)	$W_{\rm tc}$ (nm)
9605	400	2.6	450	0	⋯	⋯	⋯	300	0.8	300
9601	400	1.0	150	10	15	0.6	95	275	0.6	250
9604	350	2.6	150	20	12	0.3	68	250	0.5	250
9605 etched	400	2.6	450	0	⋯	⋯	⋯	60	0.8	⋯
9601 etched	400	1.0	150	10	15	0.6	95	60	0.6	⋯
9604 etched	350	2.6	150	20	12	0.3	68	60	0.5	⋯

Downloaded 29 Mar 2001 to 131.96.4.154. Redistribution subject to AIP copyright, see http://ojps.aip.org/japo/japcr.jsp

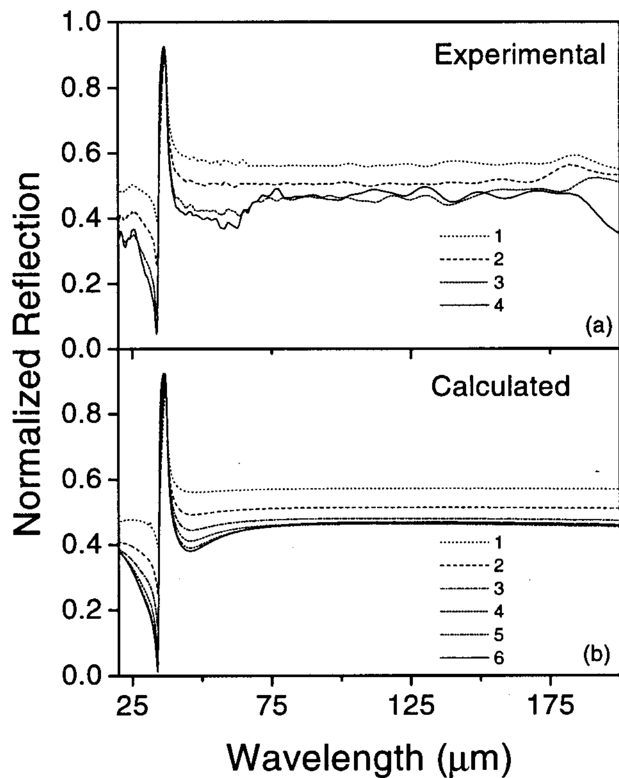

FIG. 1. Normalized reflection for 280-nm-thick GaAs:C layer on a 350-μm-thick semi-insulating GaAs substrate for different doping concentrations in the epilayer (for light incident on the doped-layer side). (a) Experimental reflection spectra for: (1) sample M7.228 with $N_p = 4.7\times10^{19}\,\mathrm{cm}^{-3}$, (2) M7.227, $N_p = 2.4\times10^{19}\,\mathrm{cm}^{-3}$, (3) M7.270, $N_p = 5.9\times10^{18}\,\mathrm{cm}^{-3}$, and (4) the 350-$\mu$m-thick SI substrate. (b) Calculated with Eq. (1) reflection for: (1) sample M7.228, (2) M7.227, (3) M7.229, (4) M7.270, (5) M7.232, and (6) the substrate. See Table I for used values of relaxation time τ. Features in experimental reflection spectra at wavelengths shorter than the reststrahlen region are due to multiphonon lattice absorption mainly in the bulk of the substrate, which is not taken into account by model Eq. (1). These features are weaker for samples with higher doping concentration, being masked by the strong reflection from the epilayer.

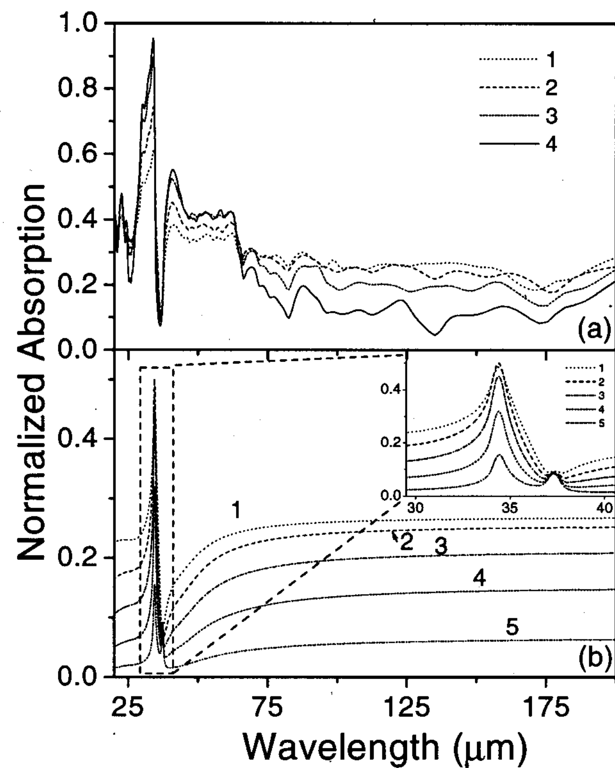

FIG. 2. Normalized absorption for 280-nm-thick GaAs:C layer on a 350-μm-thick semi-insulating GaAs substrate for different doping concentrations in the epilayer (for light incident on the doped-layer side). (a) Experimental absorption spectra for: (1) sample M7.228, (2) M7.227, (3) M7.270, and (4) a piece of the substrate. (b) Calculated absorption in the epilayer for: (1) sample M7.228, (2) M7.227, (3) M7.229, (4) M7.270, (5) M7.232, and (6) a piece of the substrate. The inset expands the 30–40 μm region, showing the free-carrier (stronger) and lattice absorption peaks in the reststrahlen region.

and magnetic fields at the interfaces of the layer with another layer. Reflection R and transmission T are calculated as the reflected and transmitted power, normalized by the incident power. The absorption is determined as $A=1-R-T$, as in the case of experiment. Absorption in each layer can also be calculated as a normalized difference between the incoming power and the outgoing power, of each layer. Interference effects arising from the reflection from the backside of the thick substrate were averaged within a spectral interval of 4 cm^{-1} modeling the experimental resolution.

IV. RESULTS AND DISCUSSION

The measured and the calculated reflection spectra for a 280-nm-thick C-doped GaAs layer on a 350-μm-thick SI GaAs substrate for five doping concentrations in the first set of samples listed in Table I are shown in Figs. 1(a) and 1(b). The experimental and calculated absorption spectra for the same set of samples are shown in Figs. 2(a) and 2(b). Calculations of reflection, transmission, and absorption were performed for measured values of layer thicknesses and concentrations. Experimental data were fitted to the calculated data using the relaxation time τ as the fitting parameter following the method of Holm, Gibson, and Palik.[10] The obtained τ values are given in Table I. Although the experimental τ values are slightly higher than the values used in the fitting, both sets show a similar decreasing trend with increasing doping concentration.

Calculated spectra are in reasonable agreement with experimental curves, with highly doped samples giving even better agreement. The reflection maximum at 37 μm and corresponding minimum in the absorption spectra are due to strong light interactions with optical phonons, and described well by the reststrahlen term in Eq. (1). Reflection from the top layer with high carrier concentration masks spectral features relating to multiphonon interactions in the bulk of the substrate. These were not taken into account in the model, since these features are much weaker than the free-carrier absorption features. Figure 3 shows the calculated absorption coefficient $\alpha=2\omega/c\,\mathrm{Im}(\sqrt{\epsilon})$ for heavily doped GaAs, with ϵ determined by Eq. (1). For the lowest measured doping concentration of $1.8\times10^{18}\,\mathrm{cm}^{-3}$ α scales with wavelength as λ^2 up to about 30 μm and reaches a maximum of $2\times10^3\,\mathrm{cm}^{-1}$ around $\lambda=120\,\mu$m. For the highest concentration level of $4.7\times10^{19}\,\mathrm{cm}^{-3}$ the λ^2 behavior is seen up to about 10 μm, and the highest value of $2.3\times10^4\,\mathrm{cm}^{-1}$ is reached at $\lambda=25\,\mu$m. Calculated (doped region) absorption curves for the C-doped samples listed in Table I are shown in

Downloaded 29 Mar 2001 to 131.96.4.154. Redistribution subject to AIP copyright, see http://ojps.aip.org/japo/japcr.jsp

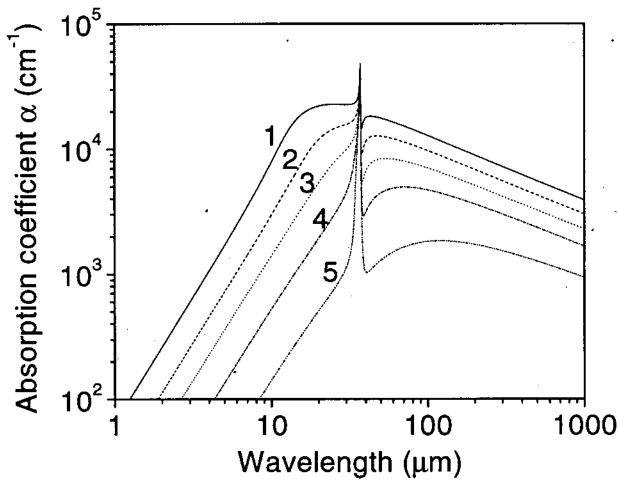

FIG. 3. Calculated absorption coefficient $\alpha = 2\omega/c\ \mathrm{Im}(\sqrt{\epsilon})$ with ϵ determined by Eq. (1) taking into account free-carrier and optical-phonon absorption, for GaAs with different doping concentrations and corresponding τ values: (1) $N_p = 4.7\times10^{19}\,\mathrm{cm}^{-3}$, $\tau = 1.2\times10^{-14}\,\mathrm{s}$, (2) $N_p = 2.4\times10^{19}\,\mathrm{cm}^{-3}$, $\tau = 1.4\times10^{-14}\,\mathrm{s}$, (3) $N_p = 1.3\times10^{19}\,\mathrm{cm}^{-3}$, $\tau = 1.5\times10^{-14}\,\mathrm{s}$, (4) $N_p = 5.9\times10^{18}\,\mathrm{cm}^{-3}$, $\tau = 1.8\times10^{-14}\,\mathrm{s}$, and (5) $N_p = 1.8\times10^{18}\,\mathrm{cm}^{-3}$, $\tau = 2.0\times10^{-14}\,\mathrm{s}$. The absorption coefficient α scales as λ^2 at shorter wavelengths (up to $\lambda \approx 10-30\,\mu\mathrm{m}$), and has a slightly decreasing tendency as wavelength increases. Sharp maximum at 37 μm is due to strong optical-phonon absorption.

Fig. 2(b). In the reststrahlen region there are two peaks of epilayer absorption shown in the inset of Fig. 2(b). The peak at the longer wavelength is practically independent of the doping concentration and corresponds to lattice absorption. The shorter wavelength peak value increases strongly with the carrier concentration and can be attributed to free-carrier absorption. The free-carrier absorption below and above the reststrahlen region increases with increasing concentration. In the long wavelength range free-carrier absorption remains significant up to 200 μm and beyond allowing the consideration of HIWIP as a prominent detection mechanism for FIR range.

Increasing the doping concentration and the emitter layer thickness is a way to increase the free carrier absorption. However, in HIWIP the doping concentration is chosen to give rise to an appropriate detector interfacial work function[7] Δ, and W_e should be of the order of inelastic scattering length $L_z \approx 20-30\,\mathrm{nm}$ for p-GaAs for optimum collection efficiency.[11] Another way is to use the resonant cavity enhanced (RCE) architecture utilizing the reflection of the incoming radiation from the bottom layer to increase the optical field intensity in the active region of the detector. The high reflection from the highly doped layer [see Fig. 1(a)] allows the use of an optically thick bottom contact layer as a mirror in the HIWIP structure. The interaction with light depends strongly on the carrier concentration and the thickness of the active layers. In the FIR range, GaAs with a doping density of $2\times10^{19}\,\mathrm{cm}^{-3}$ has a skin depth $\delta' = c/\omega\,\mathrm{Im}(\sqrt{\epsilon})$ of the order of 1 μm. Hence a typical 700 nm, bottom contact region doped to $2\times10^{19}\,\mathrm{cm}^{-3}$ will reflect back a significant fraction of the incident radiation to form a standing wave greatly reducing the electric field at the bottom contact. Since the emitter layers are optically thin (i.e., $W_e \ll \lambda_s,\ \delta$), the absorption depends on the amplitude of electric field and hence on the distance from the bottom contact layer which plays the role of the "mirror."

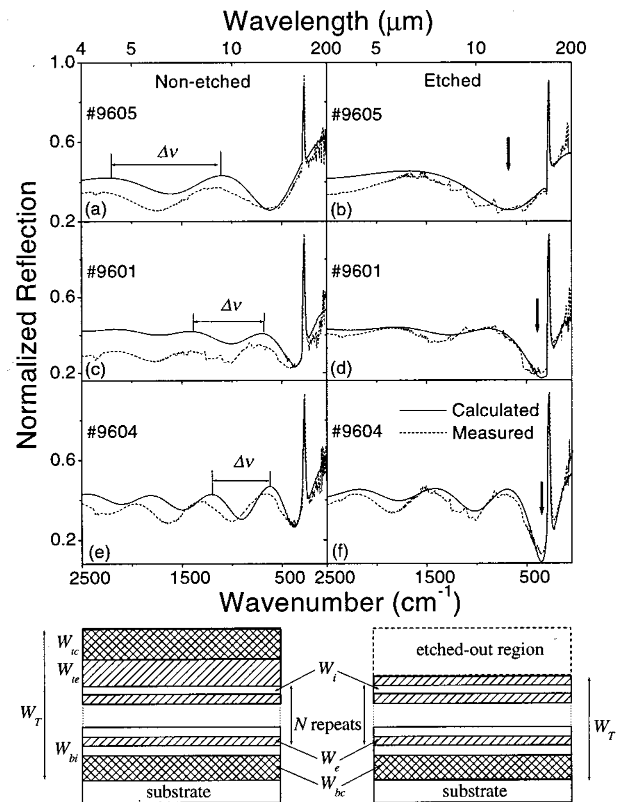

FIG. 4. Calculated (solid lines) and measured (dash lines) reflection for Be-doped multilayer detector (see Ref. 7) structures with and without the top contact, i.e., nonetched and etched: (a) nonetched 9605 with top emitter, (b) top contact removed, i.e., etched 9605, (c) nonetched 9601 with ten periods, (d) etched 9601, (e) nonetched 9604 with 20 periods of i-region-emitter, and (f) etched 9604. The nonetched and etched structures are schematically shown in the bottom part of the figure. The discrepancy for non-etched 9604 is due to 7% deviation in growth thickness. Reflection far away from the reststrahlen region is a quasiperiodic function of wave number with the period $\Delta\nu$, due to Fabry-Pérot resonator formed by the bottom contact layer and the top highly doped region. $\Delta\nu$ is inversely proportional to the thickness W_T and increases with reducing the number of $i-p^+$ repeats (from the bottom to the top), and with etching (from left to right).

Both measured and calculated reflection curves for samples in Table II are shown in Fig. 4. It is clearly seen that Eq. (1) adequately describes the spectral behavior of the multilayer HIWIP structures. The fitting parameter (τ) values of 1.2×10^{-14}, 1.5×10^{-14}, and $2.0\times10^{-14}\,\mathrm{s}$ were used for Be-doped GaAs regions with concentrations of 2.6×10^{19}, 1.0×10^{19}, and $(3-6)\times10^{18}\,\mathrm{cm}^{-3}$, respectively. All the structures demonstrate a significant resonance cavity effect due to reflection from the bottom contact layer with spectral features corresponding to their geometrical parameters. The quasiperiodic structure of a normalized reflection as a function of wave number above the reststrahlen region is seen in Fig. 4. The period $\Delta\nu$ is inversely proportional to W_T, where W_T is the total growth thickness or the distance from the highly doped top region to the bottom contact layer: $\Delta\nu \sim (2\sqrt{\epsilon_\infty}W_T)^{-1}$. Both measured and calculated $\Delta\nu$ values are presented in Table III. The discrepancy between calcu-

Downloaded 29 Mar 2001 to 131.96.4.154. Redistribution subject to AIP copyright, see http://ojps.aip.org/japo/japcr.jsp

TABLE III. Total thickness W_T and interference oscillation period $\Delta\nu$ for three nonetched (set 2) and three etched (set 3) *p*-GaAs HIWIP FIR detector structures. Here, $W_T = W_{bc} + W_{bi} + N(W_e + W_i) + W_{te} + W_{tc}$—see Table II for the parameters ($W_{tc} = 0$ for the etched structures). Reflection from the structure is a quasiperiodic function of wave number (frequency) as shown in Fig. 4 due to the optical cavity effect. The period $\Delta\nu$ is inversely proportional to cavity thickness W_T.

Sample No.	W_T (μm)	Measured $\Delta\nu$ (cm^{-1})	Calculated $\Delta\nu$ (cm^{-1})
9605	1.45	1140	1150
9601	2.20	720	720
9604	2.60	625	580
9605 etched	0.91	1920	1980
9601 etched	1.71	940	940
9604 etched	2.16	720	720

lated and measured $\Delta\nu$ values for nonetched 9604 could be explained by a 7% deviation in growth thickness according to the position of the sample from the wafer center.

The structures with greater number of internal emitters are thicker, and hence the period $\Delta\nu$ is shorter as seen in Fig. 4 ($\Delta\nu$ decreases from top to bottom). The value of $\Delta\nu$ is also less for nonetched structures [see Figs. 4(a), 4(c), and 4(e) in comparison with Figs. 4(b), 4(d), and 4(f), respectively], because the cavity in this case is formed by the bottom and the top contact layers. This distance (W_T) is greater in the nonetched case than W_T in the case of etched structures. The ''oscillations'' are weaker for both etched and nonetched 9601 structures due to lower concentration of the bottom contact region. As shown for the set of samples in Table I (see Fig. 1), reflection is weaker for low doping concentrations, and hence the interference effect is weaker.

Calculated absorption in the top emitter regions for three etched structures is shown in Fig. 5 as a function of wavelength. For the etched structures the position of the longest-wavelength absorption maximum [or the longest-wavelength reflection minimum as indicated with arrows in Figs. 4(b), 4(d), and 4(f)] corresponds to the condition $W_T \sim \lambda_s/4$. Here λ_s is the wavelength inside the medium and W_T is the total thickness of the structure. For studied structures, this condition is realized at 12, 23, and 29 μm for $W_T = 0.91$, 1.71, and 2.16 μm, respectively, falling close to the reststrahlen region, as seen in Fig. 5. To shift the absorption maximum further into the far infrared range, the total thickness W_T needs to be increased further. Compared to the etched structures, in nonetched structures, the longest-wavelength absorption maximum tends to satisfy the $W_T \sim \lambda_s/2$ condition due to the strong reflection from both top and bottom contact layers producing a better quality Fabry-Pérot resonator. It is shown that for longer wavelengths (beyond the reststrahlen wavelength region) free-carrier absorption in the top emitter region for etched structures increases with increasing the distance W_T until W_T reaches $\lambda_s/4$. This is due to the increase in the optical electric field amplitude of the standing wave as the distance from the mirror/emitter increases. For three different detector structures with $W_T = 0.91$, 1.71, and 2.16 μm, the calculated absorption (at 50 μm) in the top emitter region was 1.5, 2.6, and 3.4%, respectively. This confirms that the absorption increases as the distance from the bottom contact to top emitter increases within a thickness of $\lambda_s/4$. The increase in the response with the number of emitter layers was experimentally demonstrated. The measured 50 μm responsivities of the HIWIP detector structures were 0.12, 1.51, and 3.10 A/W for $W_T = 0.91$, 1.71, and 2.16 μm, respectively, giving the highest value for $W_T = 2.16\,\mu$m, Be-doped 20 layer (9604) HIWIP detector with λ_c of 100 μm.[12] The detector with the lowest W_T value shows a lower responsivity than expected from the calculation indicating the effect of bias field redistribution inside the illuminated multilayer structures.[13] To extend the HIWIP response to longer wavelength up to 200 μm and beyond and to improve the performance, it is necessary to design RCE structures with increased distance up to several micrometers from the bottom contact layer to the top emitter, and increased doping concentration in the emitter region.

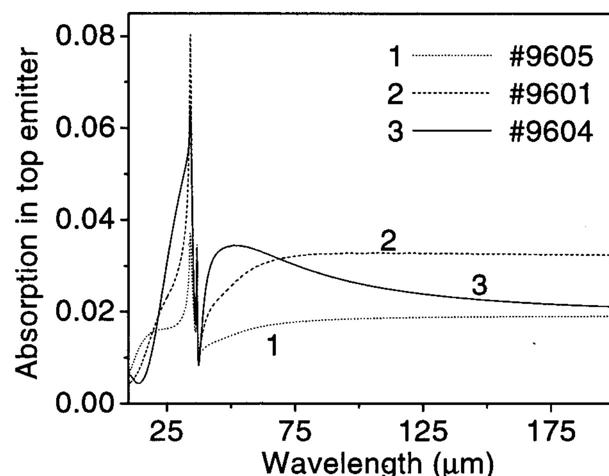

FIG. 5. Calculated absorption in the top emitter region as a function of wavelength for three etched structures: (1) 9605, (2) 9601, and (3) 9604. The first emitter region furthest from the bottom contact (9604) has the highest absorption at 50 μm. At longer than 70 μm wavelengths, emitter absorption in the sample 9601 is higher than in other samples due to lower doping concentration N_c in the bottom contact for this sample, weaker reflection, and hence higher optical electric field amplitude in the nearest vicinity of the bottom contact surface. For all these samples the position of resonant absorption, corresponding to the condition $W_T \sim \lambda_s/4$, falls close to the reststrahlen region. To shift it into the far infrared range further increasing W_T is necessary.

V. CONCLUSIONS

It is shown that the simple model of free-carrier absorption [see Eq. (1)] is in good qualitative and quantitative agreement with the experimental data for both C- and Be-doped multilayer GaAs structures with highly doped regions. Free carrier absorption in highly doped regions remains significant for wavelengths up to 200 μm and beyond giving rise to the possibility of extending the wavelength range of HIWIP detectors into FIR range. The high FIR reflection from the thick layer of highly doped GaAs allows the use of a bottom contact in HIWIP detector structure as a mirror in optical cavity architecture, significantly increasing absorption in emitter regions and hence the detector responsivity.

Downloaded 29 Mar 2001 to 131.96.4.154. Redistribution subject to AIP copyright, see http://ojps.aip.org/japo/japcr.jsp

ACKNOWLEDGMENTS

This work was supported in part by NASA under Contract No. NAG5-4950, and DND. The authors acknowledge the contributions made by M. Gao and S. Rolfe at NRC in sample preparation and SIMS measurements.

[1] R. Braunstein, J. Phys. Chem. Solids **8**, 280 (1959).
[2] R. Braunstein and E. O. Kane, J. Phys. Chem. Solids **23**, 1423 (1962).
[3] J. L. Lievin and F. Alexandre, Electron. Lett. **21**, 413 (1985).
[4] M. L. Huberman, A. Ksendzov, A. Larsson, R. Terhune, and J. Maserjian, Phys. Rev. B **44**, 1128 (1991).
[5] W. Z. Shen, A. G. U. Perera, S. K. Gamage, H. X. Yuan, H. C. Liu, M. Buchanan, and W. J. Schaff, Infrared Phys. Technol. **38**, 133 (1997).
[6] A. G. U. Perera, in *Physics of Thin Films*, edited by M. H. Francombe and J. L. Vossen (Academic, New York, 1995), Vol. 21, pp. 1–75.
[7] A. G. U. Perera and W. Z. Shen, Opto-Electron. Rev. **7**, 153 (1999).
[8] J. S. Blakemore, J. Appl. Phys. **53**, R123 (1982).
[9] A. A. Kukharskii, Solid State Commun. **13**, 1761 (1973).
[10] R. T. Holm, J. W. Gibson, and E. D. Palik, J. Appl. Phys. **48**, 212 (1977).
[11] J. Maserjian, Proc. SPIE **1540**, 127 (1991).
[12] W. Z. Shen, A. G. U. Perera, H. C. Liu, M. Buchanan, and W. J. Schaff, Appl. Phys. Lett. **71**, 2677 (1997).
[13] M. Ershov, H. C. Liu, M. Buchanan, Z. R. Wasilewski, and V. Ryzhii, Appl. Phys. Lett. **70**, 414 (1997).

Downloaded 29 Mar 2001 to 131.96.4.154. Redistribution subject to AIP copyright, see http://ojps.aip.org/japo/japcr.jsp